

Article

# Laboratory and Physical Prototype Tests for the Investigation of Hydraulic Hysteresis of Pyroclastic Soils

Marianna Pirone <sup>1,\*</sup>, Alfredo Reder <sup>2</sup>, Guido Rianna <sup>2</sup>, Luca Pagano <sup>1</sup>,  
Marco Valerio Nicotera <sup>1</sup> and Gianfranco Urciuoli <sup>1</sup>

<sup>1</sup> Dipartimento di Ingegneria Civile, Edile ed Ambientale (DICEA), Università di Napoli Federico II, Via Claudio 21, 80125 Napoli, Italy; lupagano@unina.it (L.P.); nicotera@unina.it (M.V.N.); gianurci@unina.it (G.U.)

<sup>2</sup> Regional Model and geo-Hydrological Impacts, Centro Euro-Mediterraneo sui Cambiamenti Climatici, Italy, Via Thomas Alva Edison, 81100 Caserta, Italy; alfredo.reder@cmcc.it (A.R.); guido.rianna@cmcc.it (G.R.)

\* Correspondence: marianna.pirone@unina.it

Received: 23 June 2020; Accepted: 13 August 2020; Published: 17 August 2020



**Abstract:** Proper soil water retention curves (SWRCs) are necessary for a fair analysis of groundwater flow in unsaturated slopes. The question is whether hydraulic parameters operating in situ can be reliably determined from laboratory tests or physical prototype models in order to interpret and predict soil water distributions in the field. In this paper, some results obtained by tests at different scales (testing on laboratory specimens and a physical prototype) are presented to explore the hydraulic behavior of pyroclastic soils. A theoretical interpretation of the observed behavior in the laboratory and using a physical prototype is proposed by adopting the hysteretic model of Lenhard and Parker. For each tested soil, the main hysteretic loop determined by interpreting experimental tests (at laboratory and prototype scales) overlaps with paths detected by coupling the field measurements of matric suction and water content collected at the site at the same depth. From these results, the physical prototype (medium scale) and the soil specimen (small scale) seem to be acceptable for determinations of SWRC, provided that the air entrapment value is well known.

**Keywords:** hydraulic soil behavior; hydraulic hysteresis; in situ monitoring; lysimeter; pyroclastic unsaturated soil

## 1. Introduction

Unsaturated soil mechanics play a significant role in many geotechnical problems, such as investigations concerning debris flow and mudflow initiation in partially saturated slopes. Since the soil matric suction has an impact on the mechanical strength of unsaturated soils, it is crucial to determine and understand the hydraulic behavior of the soil [1]. Therefore, the correct choice of soil water retention curves (SWRCs) and hydraulic conductivity functions (HCFs) to model soil water fluxes is crucial for carrying out reliable predictions of triggering mechanisms [2,3]. In particular, an SWRC establishes the water content change that has to occur as a result of a given matric suction change in adsorption or desorption processes. It is usually presented as a relationship between water content (gravimetric or volumetric) or the degree of saturation against soil matric suction. The shapes of SWRCs and matric suction values could vary significantly according to the void ratio, soil structure, stress history, and stress state [1]. Another crucial feature of an SWRC is its hysteretic character: the main curves for wetting and drying are not reversible. Hysteresis in the hydraulic properties can strongly affect the water flow regime; neglecting it can cause considerable errors in mass flux calculations [4].

The hydraulic properties should be determined at the scale of the modeled process; in particular, the sample should at least be large enough to encompass the representative elementary volume [5]. In this regard, on-site tests are rarely carried out because they are time-consuming, costly, and difficult to implement. In fact, they require water content and pore water pressure measurements in poorly accessible places and adequate time and geometric resolution, thus turning out to be unfeasible when the analysis spans over a very large area.

On the other hand, determinations by laboratory tests on soil specimens and on physical prototypes are simpler than those in the field, but their validity is affected by scale troubles due to a reduced sample size that is often inadequate to incorporate soil heterogeneity, especially if hydraulic conductivity is of interest [6]. The significance of small- and medium-scale measurements to provide information about large-scale flow behavior is largely debated in the literature [1–4,6]. Comparison between field and laboratory data has been investigated by many authors [1–3,7,8], and non-matching hydraulic functions have been justified by invoking differences in terms of (i) representativeness of the sample (specimen or physical prototype); (ii) space–time resolution of field and laboratory measurements; (iii) affinity between boundary conditions in the field and those applied to the soil core and to the physical prototype; and (iv) procedures for mathematical interpretation. In addition, some discrepancies between methods adopted to investigate hydraulic properties can arise from so-called ‘dynamic effects’ that may occur during transient water flow. In fact, ‘dynamic nonequilibrium’ provides for a dependence of hydraulic properties on flow-rate or local nonequilibrium between water content and pressure head, even in the case of a process of imbibition or drainage that develops monotonically [9,10].

Within this framework, the aim of this work was to investigate the hydraulic hysteresis of pyroclastic soils at different scales by pointing out consistencies and discrepancies in SWRC trends and factors that may have determined some of the resulting differences. In particular, this paper compared SWRCs obtained for unsaturated pyroclastic soil by laboratory tests (small scale) and physical prototype tests (medium scale). The ashy soils composing the top and the deep soil layers of a slope monitored at a test site (Monteforte Irpino, Southern Italy) [7,11,12] were tested at small and medium scales, respectively [13–16].

This paper first provides a brief description of the test site and tested soil (Section 2.1). Following that, it illustrates the experimental procedures followed for small- and medium-scale tests (Sections 2.2 and 2.3) and theoretical procedures adopted to mathematically describe the retention behavior (Section 2.4). In particular, at both test scales, the main drying curves and secondary drying/wetting branches were experimentally obtained. Furthermore, the model of Parker and Lenhard [17] was adopted to interpret the hydraulic hysteresis, adapting the classical van Genuchten equation to the main and scanning paths [18]. The results are extensively reported in Section 3.

The main loop and secondary paths modeled for each soil tested were compared to paths obtained by coupling field measurements of matric suction and volumetric water content; the aim of the comparison was to test the reliability of the hydraulic characterization determined at small and medium scales for capturing field hydraulic behavior. The discussion on the comparison between the paths on the SWRC plane determined at different scales is included in Section 4.

## 2. Materials and Methods

### 2.1. The Test Site and the Soil Physical Properties

The tested soil was collected at a test site located at Monteforte Irpino, about 40 km east of Naples, in Southern Italy. The test site was selected as a representative of other pyroclastic slopes in Campania subjected to rapid landslides (e.g., Pizzo D’Alvano, Monti di Avella, and Monte Partenio) (Figure 1a). The stratigraphic profile consists of an unsaturated pyroclastic soil cover a few meters thick (3–5 m), deposited by a series of eruptions of Mt. Somma–Vesuvius on top of a limestone bedrock (Figure 1b). The test site was monitored from 2006 to 2012. The monitoring equipment consisted of (i) 94 traditional

vacuum tensiometers; (ii) 40 TDR (Time Domain Reflectometry) probes with triple needles 15 cm long; (iii) 6 Casagrande piezometers; and (iv) a weather station.

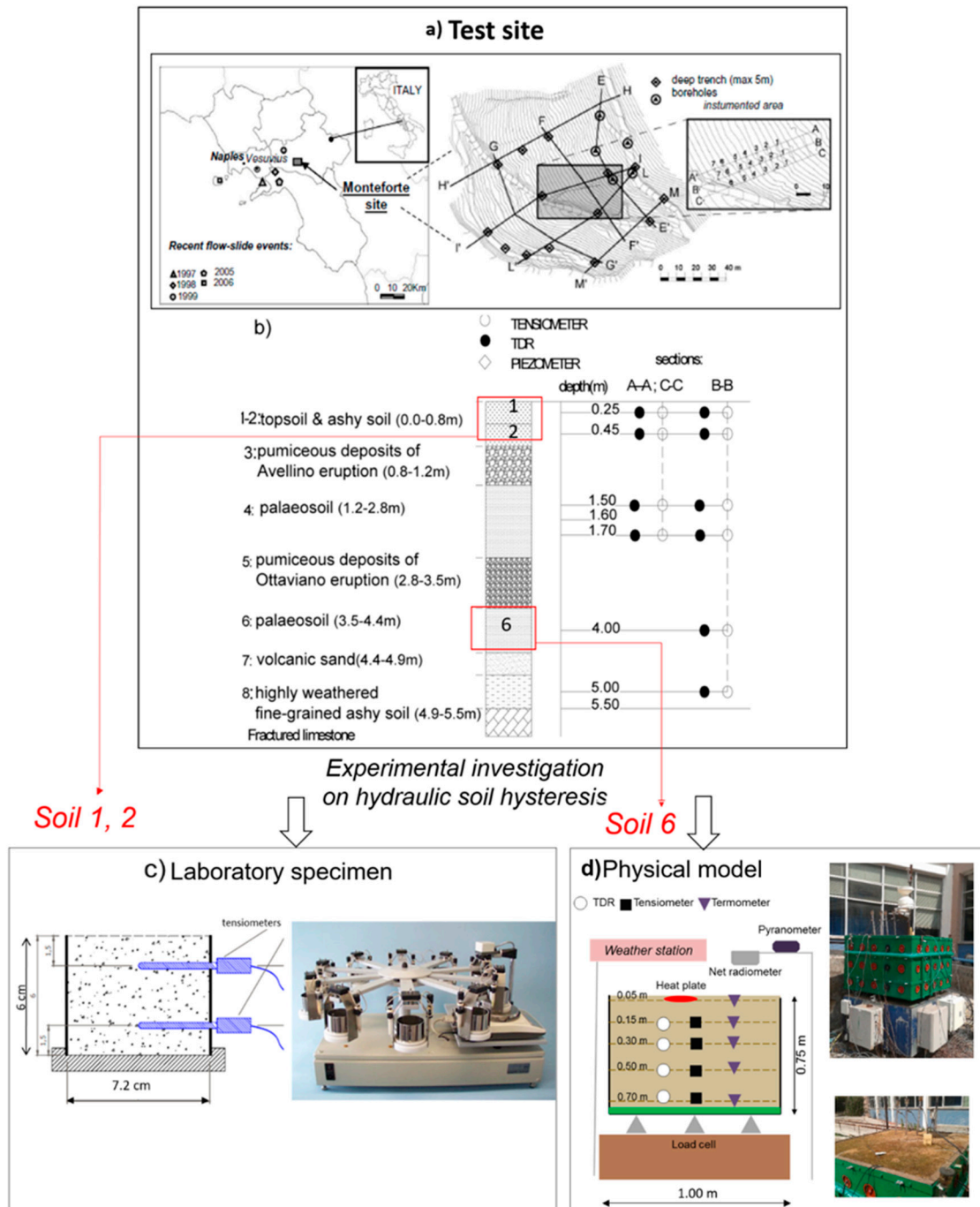


**Figure 1.** (a) The test site of Monteforte Irpino (Southern Italy); map with indications of trenches and boreholes; and (b) simplified stratigraphic soil profile with the layout of the instrumentation installed along each monitored vertical section along section B–B'. Methods adopted to test the hydraulic soil properties: (c) evaporation and imbibition tests on soil specimens (investigation at a small scale); and (d) monitoring of the physical prototype (investigation at a medium scale).

Tensiometers were installed at different depths in all the vertical sections, and TDR and Casagrande piezometers were installed in the vertical sections distributed along the central section, B–B<sub>0</sub> (Figure 1a,b). Measurements of matric suction and volumetric water content were collected every week, and the

meteorological data were registered by datalogger every four hours. However, the test site itself has been extensively described elsewhere; readers can refer to [7,11,12,19,20] for further detailed information about the instrumented area.

In this study, the hydraulic characterization of topsoil (named soils 1 and 2 in Figure 1b) and of deep soil (named soil 6 in Figure 1b) collected at the test site is investigated.

In Table 1, the mean physical properties of the tested soils are reported. For all soils, the porosity is very high (0.7 on average). The envelope of grain size distributions of several samples taken for soil testing is shown in Figure 2. Shallower soils (1 and 2) have a fairly similar grain size envelope: the two envelopes are partially overlapping. Soils 1 and 2 are silty sands, while Soil 6 contains a larger percentage of fine soils. Soils 1 and 2 were tested at the scale of the soil specimen (i.e., working a total volume of about 0.24 dm<sup>3</sup>), while soil 6 was tested at the scale of the physical prototype (i.e., 1 m<sup>3</sup>); in the first case, undisturbed soil specimens were tested, and, in the second case, soil samples were reconstituted at the same field porosity.

**Table 1.** Mean physical properties of tested soils, sample sizes, and adopted methods.

Soil	n	$\gamma_d$ (kN/m <sup>3</sup> )	G <sub>s</sub>	Size of Sample (d*; h**) (cm)	Testing Method
1 (topsoil)	0.66	7.90	2.65	soil specimen (d: 7.2; h: 6)	evaporation/imbibition test
2 (topsoil)	0.69	7.90	2.55	soil specimen (d: 7.2; h: 6)	evaporation/imbibition test
6 (deep soil)	0.72	7.13	2.57	physical prototype (d: 115; h: 75)	monitoring of soil hydraulic behavior under actual weather forcing [13–16]

d\*: diameter of cylindrical sample. h\*\*: height of cylindrical sample.

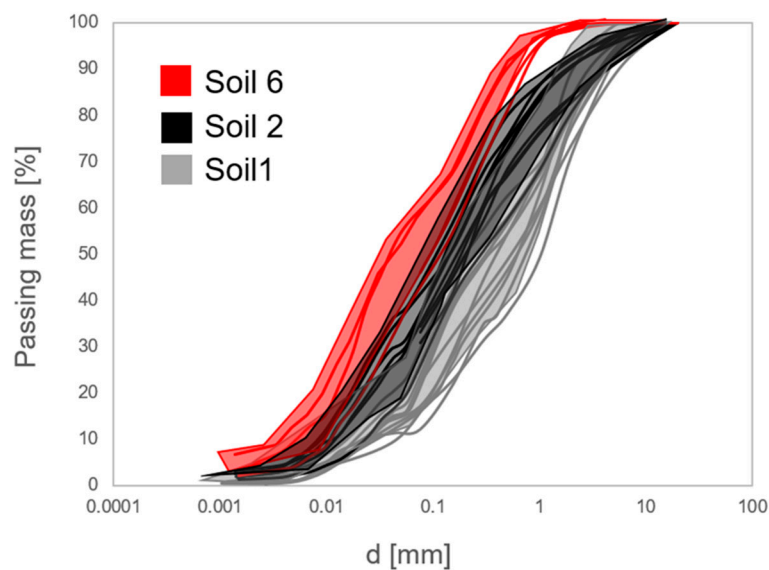


**Figure 2.** Grain size distributions of the soil tested: soils 1 and 2; soil 6.

At the laboratory, the soil specimens of soils 1 and 2 were subjected to simple controlled paths of evaporation and wetting; in particular, the wetting phases were carried out step by step, reaching quasi-steady conditions at the end of each step. On the contrary, soil 6, which filled the lysimeter, was exposed to the atmosphere and, thus, subjected to transient and not artificially imposed boundary conditions.

The main features concerning the size of the sample tested and the method adopted to determine the hydraulic behavior are summarized in Table 1.

## 2.2. Investigation at the Small Scale: Laboratory Test

The investigation at the small scale involved soils 1 and 2 and consisted of a sequence of testing phases: a constant head permeation test, a forced evaporation test followed by several wetting–drying cycles and, finally, a drying test in a pressure plate apparatus. The soil specimen was 6 cm in height and 7.2 cm in diameter.

The forced evaporation, along with the wetting and drying cycles, was carried out in a ku-pf MP10 apparatus (Umwelt-Geräte-Technik GmbH, Müncheberg, Germany) (Figure 1c). The equipment consists of a star-shaped sampler changer. Each changer arm holds a metallic basket, in which the specimen is laid, equipped with two mini-tensiometers connected to a conditioning unit (in which matric suction measurement resolution is 0.01 kPa). After saturation and the permeability test, the specimen was installed in the baskets. A plastic paraffin film (Parafilm M) was fixed at the bottom of the specimen to prevent water evaporation and drainage using the O-ring of the base support. Additionally, at the upper part of the specimen, cling film, as well as a metallic cap, was added at the start of the test to reach the hydrostatic conditions throughout the sample and during the wetting phase after adding water to prevent evaporation. The basket was installed in a rotating changer arm and was weighed every 10 min on a precision scale with a resolution of 0.01 g to register variations in water content. The maximum value of matric suction measured by the mini-tensiometer was 90 kPa. More details about the ku-pf MP10 apparatus are reported in Nicotera et al. [19], where the experimental procedure to perform and to interpret the evaporation tests are extensively discussed. Here, the research was extended to wetting paths.

Evaporation and imbibition processes were recorded in the ku-pf apparatus during the cycles of drying and wetting phases. In the drying phase, the water was allowed to evaporate from the upper surface of the specimen. The evaporation was initiated by removing the top sealing cap and the cling film from the specimen once a hydrostatic pressure distribution, detected via mini-tensiometers, had been reached. The wetting phase consisted of repeatedly pouring a fixed quantity of distilled water onto the top surface of the specimen and allowing it to infiltrate and redistribute within the soil. The top cap and cling film were removed while water was poured, but they were replaced immediately after, during infiltration and redistribution, to prevent water evaporation. If the matric suction values measured by both tensiometers exceeded 15 kPa, 5 g (equivalent water layer thickness of 0.12 cm) of water was applied to the top of the specimen. However, in order to obtain more refined data near the air-entry value (AEV) of the SWRC, 3 g (equivalent water layer thickness of 0.07 cm) of water instead of 5 was added. Each new wetting step was initiated after the measured matric suction indicated that a hydrostatic pore water pressure distribution was reached. Each wetting step lasted for at least two hours.

It is useful to point out that the procedure discussed in this study does not measure the soil volume variation. It is well known that some soil types undergo volume changes due to the suction variation during the SWRC test, such as expansive and collapsible soils. In these cases, it is essential that such changes in the void ratio are taken into account to properly determine the SWRC in terms of the degree of saturation and volumetric water content, as stated by many authors [21–29].

However, previous experimental studies (oedometer tests in natural conditions and at full saturation) have demonstrated that (i) the topsoil of the test site (soils 1 and 2) is over-consolidated and, thus, quite rigid: in fact, it is frequently subjected to large changes in suction due to the interaction between the atmosphere and soils; and (ii) the volume changes due to water content variations (resetting matric suction to zero) in pyroclastic soils of this region are nonsignificant [30,31].

## 2.3. Investigation at the Medium Scale: Lysimeter

The measurements of matric suction and volumetric water content from the monitoring of a physical prototype were used to investigate the hydraulic soil behavior at the medium scale.

The physical prototype consists of a lysimeter, a tank ( $1.15 \times 1.15 \times 0.75$  m) made of 3 cm thick wooden boards containing a pyroclastic soil layer of  $1 \text{ m}^3$ . It was exposed to the atmosphere at a site in

Napoli (Italy). The pyroclastic soil is a silty sand sampled from the Monteforte Irpino test site at a depth of 3.30 from the ground surface (i.e., soil 6). The finest component of such a soil (silt with some clay) is non-plastic due to the absence of active minerals. Grain size distribution and field porosity of such a silty sand are very similar to those of other mantling Campanian slopes, including those of Nocera Inferiore (Lattari Mts.), which was involved in a rainfall-induced landslide in 2005 [32].

Operationally, the layer was reconstituted in the tank using dry pluvial deposition. The aim was to return a low soil density comparable to those retrievable in situ [33]. Oven-dried material was placed within the tank by using a filling funnel perpendicularly and slowly moved to the soil surface. A constant fall height (space between funnel and soil surface) was maintained and limited, while the diameter of the rigid tube (8 cm) ensured high deposition intensity. Both measures permit the attainment of high final soil porosities (about 70%). Since its deposition (May 2010), the layer has been exposed to the atmosphere for ten hydrological years (Figure 1d).

During the timespan of September 2010–August 2014 (four hydrological years), the layer surface was bare. Then, at the end of the fourth hydrological year (beginning of September), the layer surface was sown with a gramineous grass (a mix of *Lolium Perenne*, *Festuca Rubra* and *Poa Pratensis*) to thoroughly investigate the effect of transpiration on the soil hydrological response. This condition was maintained up to January 2020.

At the lysimeter boundaries, different conditions act at:

- the uppermost surface, where there are inward (rainfall infiltration) and outward (evaporation) water flows due to the interaction between the atmosphere and topsoil; both flows were monitored by regularly weighing the tank through three load cells that were used to quantify water storage changes, which, in turn, corresponded to rainfall infiltration amounts during periods without drainage and actual evaporation during periods without drainage or rainfall;
- the bottom, where there is a seepage surface due to the capillary barrier effect regulated by a geotextile interposed between the layer and the holed tank base; the seepage surface behaves as an impervious surface, while negative pore water pressures act near the surface and as a free draining surface otherwise; in this regard, the experimental results can be retrieved in [34]; and
- the lateral faces, where surfaces are impervious to water flow.

In addition to the load cells, the lysimeter was also instrumented to record the main weather variables (rainfall, air temperature, air relative humidity, and wind velocity and direction), some physical variables relating to energy balance at the soil–atmosphere interface (solar and net radiation, soil heat flux) and hydrological and thermal variables (matric suction, volumetric water content and temperature) within the layer. As for the last variable type, matric suction, volumetric water content, and temperature were monitored at four depths (15, 30, 50, 70 cm) separately through jet-fill, TDR probes, and thermistors (temperature was also monitored at 5 cm) (Figure 1d).

All measurements were collected through two CR1000 control units from Campbell Scientific (Logan, Utah, USA) with a frequency between 20 s (e.g., load cells) and 15 min (e.g., weather variables). Jet-fill tensiometers and TDR probes were collected at a frequency of 5 min. All measurements were processed at an hourly scale. Load cell measurements were processed using a trimmed mean (25th–75th percentiles) to avoid any outliers attributable to experimental errors.

The main results of monitoring performed over several years are reported in Reference [13–16]. In this work, measurements collected over the first four hydrological years are accounted for.

#### 2.4. Modeling Methods

The experimental paths detected in the soil water retention plane were modeled using the hysteretic model proposed by Lenhard et al. (1991) [35] as a special case for two fluids defined by the Lenhard and Parker [36] and Parker and Lenhard (1987) [17] models, here indicated as the LP model.

The approach shapes the main drying and wetting branches of the SWRC by adopting the van Genuchten [18] equation, but each branch is characterized by its own fitting parameters, reported in

Equations (1) and (2). The choice of the van Genuchten equation is supported by the good fit of the main drying curves determined in the lab on soils, and those tested here are similar to those obtained by Nicotera et al. [19] and Dias [37]. However, the model based on further modifications of the van Genuchten equation [38,39] could provide more reliable predictions of hydraulic conductivity function, but, unfortunately, there are no available measurements of unsaturated conductivity on these soils.

In Equations (1) and (2), the superscripts  $d$  and  $w$  refer to the main drying and main wetting curves, respectively,  $\theta$  is the volumetric water content, and  $s$  is the matric suction. However, the PL model reduces the number of these parameters by relying on the assumptions that the residual water content  $\theta_r$  and coefficient  $n$  of these two curves are the same ( $\theta_r^d = \theta_r^w = \theta_r$ ;  $n_d = n_w = n_v$ ), while values of the saturated volumetric water content  $\theta_s$  and coefficient  $a$  are potentially considered to be different (with  $\theta_s^d$  being higher than or equal to  $\theta_s^w$ , and  $a^d$  being less than or equal to  $a^w$ ), also accounting for the effect of the air entrapped that may occur during the wetting process when zero matric suction is drawn in conditions with less than full saturation.

$$\theta(s) = \theta_r + \frac{\theta_s^d - \theta_r}{\left[1 + (\alpha^d s)^{n_v}\right]^{\left(1 - \frac{1}{n_v}\right)}}, \quad (1)$$

$$\theta(s) = \theta_r + \frac{\theta_s^w - \theta_r}{\left[1 + (\alpha^w s)^{n_v}\right]^{\left(1 - \frac{1}{n_v}\right)}}. \quad (2)$$

The scanning paths were scaled from the main branches following the method presented by Parker and Lenhard [17]. Compared with other models based on a scaling procedure [40,41], this model allows for the prevention of artificial pumping errors, that is, the non-closure of the scanning loops in simulated cyclic paths, which is considered to be an aberration rather than a soil property [42]. This is avoided in the model by collecting all the reversal points experienced by the soil. Preserving the “memory” of the various wetting–drying cycles to which the sample has been subjected allows paths to draw closed scanning loops. The LP model adopts the Land approach [43] for estimation of the air entrapment effect for two different water contents at saturation: one for the main drying ( $\theta_s^d$ ) curve and another one for the main wetting ( $\theta_s^w$ ) curve.

The hydraulic conductivity function (HCF) is described by Equation (3) [18,44], where  $K(s)$  is the soil hydraulic conductivity, and  $l$  and  $m$  are fitting parameters, in which  $m = 1 - 1/n_v$ ,  $S$  is the effective degree of saturation (Equation (4)), and  $K_{sat}$  is the saturated hydraulic conductivity.

$$K(s) = K_{sat} S^l \left(1 - \left(1 - S^{1/m}\right)^m\right)^2, \quad (3)$$

$$S = \frac{\theta - \theta_r}{\theta_s^d - \theta_r}. \quad (4)$$

Similarly, to account for air entrapment, this formulation for HCF was modified by Lenhard and Parker [36]. The model adopted here considers hysteresis in  $K(s)$ , not in  $K(\theta)$ .

The LP model was implemented in the software HYDRUS-1D, which numerically solves [45] the Richards' equation using standard Galerkin-type linear finite element schemes. The code is able to simulate the water movement in one-dimensional variably saturated media. Therefore, the fitting of experimental data of the hysteretic model was carried out by means of inverse analysis operating in two phases because of the large number of parameters. The first phase involved the parameter vector  $(\theta_s^d, \theta_r, \alpha^d, n, l)$  associated with the main drying branch; the second phase was treated with the parameter vector  $(\theta_s^w, \alpha^w)$  associated with the main wetting branch. The inverse analysis was carried out using the software HYDRUS-1D, in which the objective function used to fit the data was minimized using the Levenberg–Marquardt nonlinear minimization method [46].

In the following two subsections, the conditions imposed on the model for fitting the experimental data from laboratory tests and from the physical prototype, respectively, are described in depth.

2.4.1. Fitting of the Experimental Data from Laboratory Tests

The fitting of the main drying curve followed the procedure defined by Nicotera et al. [19], after some modifications. The initial condition was fixed as the hydrostatic pressure distribution estimated from initial suction measurements (Figure 3a). The water flow occurring within the specimen was vertical, with a null flux at the bottom and an upward flux at the upper boundary equal to the weight change in the specimen in the given time range. Data sets and respective weights in the objective function were composed of (i) matric suction measurements at the tensiometers during the monitoring time, with a weight of 1; (ii) the pair  $(s, \theta)$  obtained from the pressure plate, with a weight of 5; and (iii) the pair  $(s, \theta)$  corresponding to the AEV, with a weight of 5. The AEV was roughly identified as the point of maximum curvature on the WRC curve, obtained by coupling the mean measured matric suction to the average water content estimated by the measured variation in the soil weight during the evaporation test. The initial estimation and range of variation in the fitting parameters were set to those suggested by Nicotera et al. [19]. Parameters  $l$ ,  $n$ , and  $\theta_r$  are the same for both branches [36].

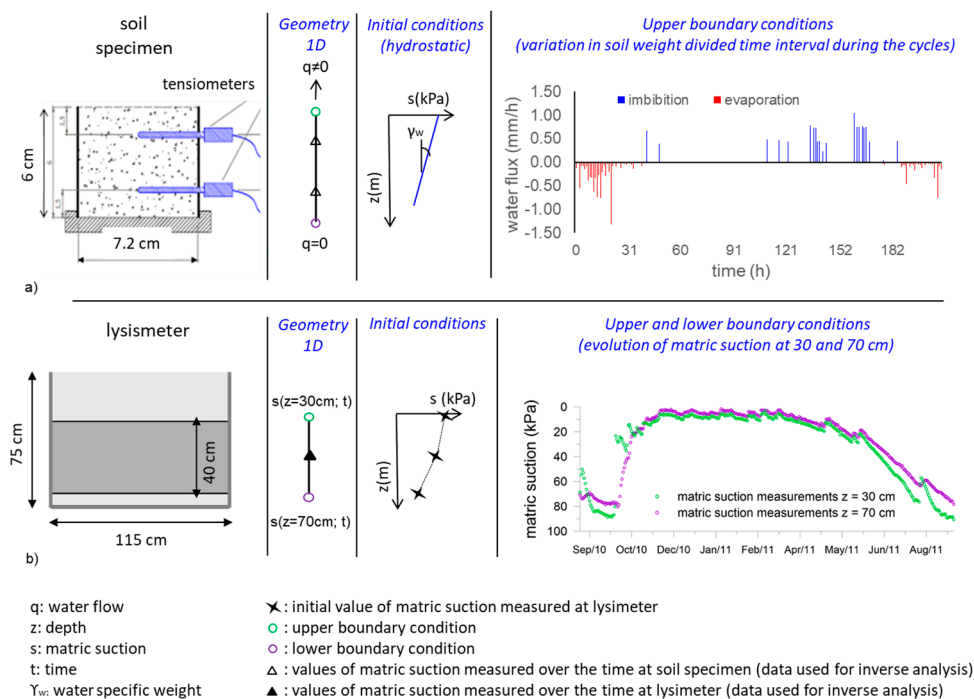


Figure 3. Geometry and initial and boundary conditions adopted in the inverse analyses: (a) soil specimen (Section 2.4.1); (b) lysimeters (Section 2.4.2).

Regarding the wetting branch, the fitted parameters were  $\theta_s^w$  and  $\alpha^w$  only. The parameter  $\theta_s^w$  was allowed to vary between 0 and  $\theta_s^d$ , and  $\alpha^w$  varied between 0 and  $100 \text{ kPa}^{-1}$ . Initial estimation of the parameter  $\theta_s^w$  was obtained from the experimental SWRC, observing the final point of the wetting path; the initial values of  $\alpha^w$  were assumed to be equal to  $2\alpha^d$ . The boundary conditions adopted for the wetting phase reproduced the variations in water content in the specimen by imposing constant fluxes of water at the upper boundary (Figure 3a). Each wetting step consisted of initial imbibition for a short time range (10 min), producing an increase in sample weight as a result of adding water. The water flow during the equalization time was estimated from variations in water content in intervals of approximately 40 min. At the lower boundary, there was a null flux of water (Figure 3a). The data set was composed of the monitored matric suction at both tensiometers. All data points were affected by the same weight, which is equal to 1 in the objective function.

#### 2.4.2. Fitting of the Experimental Data from the Physical Prototype

The suction–water content pairs measured during the monitoring period (2010–2014) were adopted to characterize soil 6 through the *PL* model [16]. The quantification of the seven parameters ( $\theta_s^d, \theta_s^w, \theta_r, \alpha^d, \alpha^w, n_v, l$ ) was carried out according to the following:

- (1)  $\theta_s^d, \theta_r, \alpha^d, n_v$  were obtained by the experimental main drying curve determined by Nicotera et al. [19];
- (2)  $l$  was assumed to be 0.5; and
- (3)  $\theta_s^w, \alpha^w$  were determined by numerically interpreting data recorded during the first year in the bare soil and were validated through the data collected in the remaining three years.

To estimate the parameters, the computational domain (Figure 3b) was fixed with respect to the soil layer included between the depths of 30 and 70 cm. Then, the suctions monitored at 30 and 70 cm acted as boundary conditions (Figure 3b), while the matric suction–volumetric water content pairs recorded at a depth of 50 cm worked as control points in the objective function. The initial condition was defined according to the three monitored suction points at 30, 50, and 70 cm. Regarding the parameters to be fitted,  $(\theta_s^w, \alpha^w)$  were allowed to vary within  $(\theta_r \theta_s^d)$  and  $(a^d 10a^d)$ , respectively. As the initial estimation,  $\theta_s^w$  was assumed to be  $0.7 \theta_s^d$ , while  $a^w$  was defined as  $2 a^d$ .

### 3. Results

#### 3.1. Investigation at the Small Scale: Laboratory Test

In Table 2, the experimental tests performed in the laboratory on soils 1 and 2 are summarized. In particular, seven tests were carried out: four tests on soil 1 (A–D) and three tests on soil 2 (E–G). The tests consisted of the following phases: (i) saturation and measurements of saturated conductivity in the permeameter; (ii) main drying, paths 1–2, obtained by imposing forced evaporation on an initially saturated soil core positioned in a ku-pF apparatus up to a maximum matric suction value of 70 kPa; (iii) a wetting–drying cycle, paths 2–4 (on soil 1) and paths 2–6 (on soil 2), obtained by progressively wetting the same soil core (by sprinkling water on the top of the sample sealed on the other sides and waiting for matric suction equalization) and then drying it again; and (iv) drying test in the Richard Plate to determine the residual soil conditions, paths 4–5 (on soil 1) and 6–7 (on soil 2). In this way, there was an attempt to reproduce in the laboratory the upper boundary condition occurring on-site, i.e., rainwater infiltration from the ground surface. In Table 2, the final values of matric suction and volumetric water content reached at the end of each phase are also reported. Furthermore, the number of stages through which the drying and wetting process is accomplished is also reported.

In Figure 4, the results of tests A and F in the ku-pF apparatus are presented as representatives of the observations made in all the tests. The specimen of soil 1 was subjected to two drying phases and one wetting phase (one cycle) (Figure 4a), while the specimen of soil 2 underwent three drying and two wetting phases (two cycles) (Figure 4b). Matric suction increased during the drying phase, while the soil weight, and thus the water content, decreased. The wetting phase consisted of a sequence of steps initiated by an abrupt increase in water content, which resulted in a sudden drop in the matric suction measured by the top tensiometer. The pressure distribution within the soil then tended toward a steady hydrostatic condition, in which the matric suction measured by the top tensiometer should be approximately 0.3 kPa higher than that measured by the bottom tensiometer. The weight of the sample during each wetting step remained constant; obviously, the water content distribution was not uniform within the soil. Matric suction values obtained by inverse analyses overlap with the measurements in Figure 4a,b. The LP model satisfactorily reproduced the cycles determined experimentally: the calculated values were in good agreement with the experimental data (Figure 4a,b). Therefore, the LP model satisfactorily reproduced the cycles determined experimentally.

**Table 2.** Tests carried out in the laboratory: saturation, evaporation, wetting, and drying cycles.

Experimental Data								
Soil	Test	Porosity		Phase	n Step <sup>o</sup>	Final State		
		#	N			#	s (kPa)	Theta
1	A	0.63		0–1	saturation	17	0.3	0.58
				1–2	evaporation		44.7	0.24
				2–3	wetting		0.5	0.54
				3–4	evaporation		16.6	0.33
				4–5	drying		1000.0	0.18
1	B	0.64		0–1	saturation	17	0.8	0.59
				1–2	evaporation		39.0	0.25
				2–3	wetting		1.4	0.52
				3–4	evaporation		14.8	0.33
				4–5	drying		1000.0	0.16
1	C	0.68		0–1	saturation	18	1.7	0.58
				1–2	evaporation		41.1	0.31
				2–3	wetting		1.71	0.57
				3–4	evaporation		22.3	0.37
				4–5	drying		1000.0	0.20
1	D	0.67		0–1	saturation	18	0.8	0.63
				1–2	evaporation		45.0	0.31
				2–3	wetting		0.6	0.60
				3–4	evaporation		21.89	0.38
				4–5	drying		1000.0	0.22
2	E	0.71		0–1	saturation	31	0.6	0.58
				1–2	evaporation		57.0	0.28
				2–3	wetting		1.0	0.56
				3–4	evaporation		56.0	0.29
				4–5	wetting		0.6	0.57
				5–6	evaporation		58.1	0.28
				6–7	drying		1000.0	0.18
2	F	0.72		0–1	saturation	38	0.8	0.62
				1–2	evaporation		61.8	0.29
				2–3	wetting		0.5	0.60
				3–4	evaporation		57.0	0.29
				4–5	wetting		0.5	0.60
				5–6	evaporation		58.0	0.29
				6–7	drying		1000	0.20
2	G	0.64		0–1	saturation	31	2.4	0.56
				1–2	evaporation		46.9	0.29
				2–3	wetting		0.7	0.57
				3–4	evaporation		58.2	0.27
				4–5	wetting		0.7	0.56
				5–6	evaporation		54.9	0.27
				6–7	drying		1000.0	0.12

The arithmetic mean of the two measurements of matric suction coupled to the average water content of the whole soil sample is reported in Figure 5a–d. This is an approximate interpretation of data used to construct SWRCs; in fact, spatial variations in water content and in matric suction inside the sample are not taken into account. These results point out that (i) the hysteresis of the second and third cycle is lower than that of the first; (ii) the matric suction value corresponding to the knee on the wetting path is lower than that on the main drying curve (entry-air suction); and (iii) the amount of entrapped air can be estimated by observing the difference in the maximum volumetric water content

measured along the main drying path and reached at the end secondary wetting path. It seems to be significant in soil 1 (Figure 5a,b; Table 2) and low or negligible in soil 2 (Figure 5c,d; Table 2).

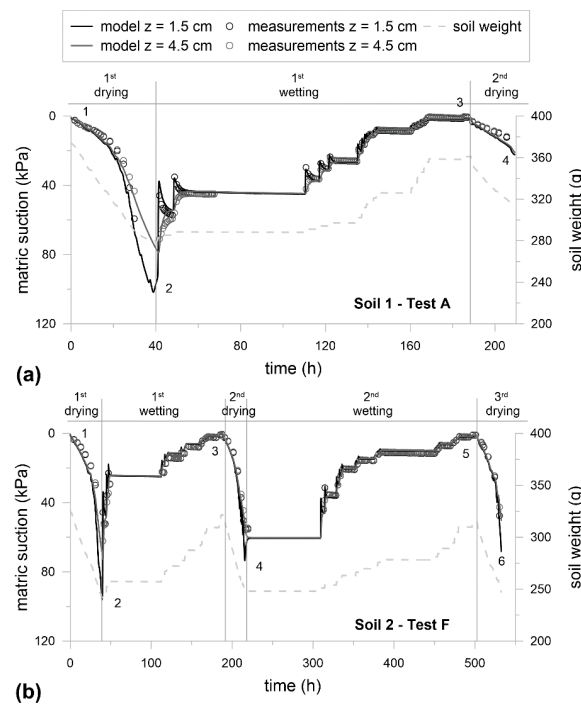


**Figure 4.** Results on soils 1 and 2 through laboratory tests (small scale). Experimental measurements of matric suction (symbols) at the top and bottom tensiometers compared to the calculated values (continuous lines) and soil weights measured over time for test A (a) and test F (b) in the ku-pF apparatus.

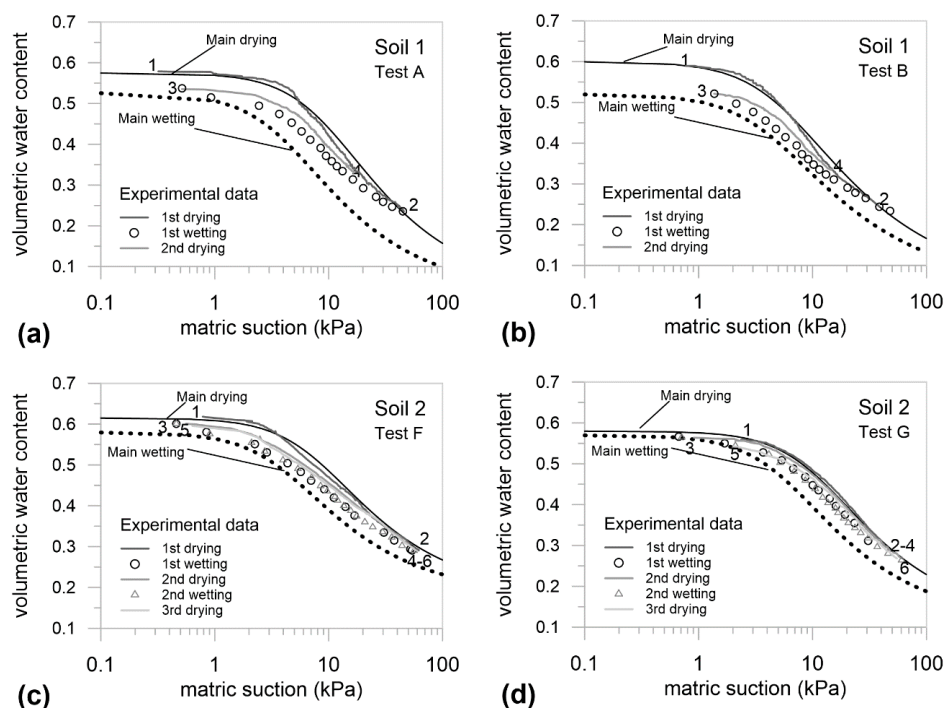


**Figure 5.** Results on soils 1 and 2 through laboratory tests (small scale). The main loop obtained from inverse analysis (main drying and main wetting) overlaps with the experimental data (main drying and wetting–drying cycles) of tests (a) A, (b) B, (c) F, and (d) G.

The fitted main drying and main wetting of SWRCs predicted by the model are also reported in Figure 5a–d. It is evident that the curve that models the main drying fits the experimental data from the first drying, and all the experimental cycles are included in the main loop. Indeed, the inverse analysis provided the parameters of the main wetting curve, which allowed the fitting of the experimental cycles to have a very high value of the coefficient of determination,  $R^2$  (Table 3).

**Table 3.** Values of Mualem–van Genuchten model parameters of the main drying and main wetting curves derived via inverse analysis of all soils tested.

Soil	Test	Ksat	$\theta_s^d$	$\theta_r$	$\alpha_d$	$n$	$l$	$\theta_s^w$	$\alpha_w$	$R^2$
		m/s			$\text{kPa}^{-1}$				$\text{kPa}^{-1}$	
1	A	$5.56 \times 10^{-6}$	0.575	0.027	0.108	1.600	−0.500	0.526	0.250	0.994
1	B	$5.56 \times 10^{-6}$	0.600	0.033	0.180	1.500	−0.500	0.520	0.240	0.990
1	C	$4.28 \times 10^{-6}$	0.600	0.200	0.105	1.860	−0.500	0.560	0.180	0.994
1	D	$4.65 \times 10^{-6}$	0.650	0.107	0.134	1.450	1.000	0.570	0.200	0.994
mean		$5.0 \times 10^{-6}$	0.61	0.09	0.13	1.60	−0.1	0.5	0.22	0.99
std		$6.5 \times 10^{-7}$	0.03	0.08	0.03	0.18	0.75	0.02	0.03	
2	E	$5.53 \times 10^{-6}$	0.589	0.19	0.095	1.8	1	0.58	0.2	0.705
2	F	$5.60 \times 10^{-6}$	0.615	0.173	0.13	1.6	1	0.58	0.25	0.963
2	G	$9.72 \times 10^{-7}$	0.59	0.103	0.099	1.59	1	0.57	0.18	0.945
mean		$4.0 \times 10^{-6}$	0.60	0.16	0.11	1.66	1.0	0.8	0.21	0.87
std		$2.6 \times 10^{-6}$	0.01	0.05	0.02	0.12	0.00	0.01	0.04	
6	Year 1	$1.0 \times 10^{-6}$	0.68	0.26	0.07	1.90	0.50	0.63	0.10	0.99

The Mualem–van Genuchten model parameters, as derived from the results of the optimization process of the first evaporation phase and then of the cycles, are reported in Table 3. The coefficient of determination ( $R^2$ ) ranges between 0.99 and 0.70. Soils 1 and 2 behave like coarse-grained materials, and the AEV ranges from 2 kPa to 6 kPa ( $\alpha_d$  varies between 0.11 and 0.13  $\text{kPa}^{-1}$ ). In order to check the reliability of the AEV, these values were compared with those detected on the gravimetric water content–suction plane by following the procedure suggested by Pasha et al. [29]. This procedure is able to minimize the possibility of missing or misrepresenting the location of the AEV without the need for measuring the volume change of the sample during the SWRC test. The values of the AEV identified according to Reference [29], which are not reported here for the sake of brevity, are very close (1 kPa higher at maximum) to those obtained by fitting the data through the Mualem–van Genuchten model on the volumetric water content–suction plane. The residual volumetric water content ( $\theta_r$ ) ranges between approximately 0.03 and 0.20 in soil 1 and between 0.10 and 0.20 in soil 2. The volumetric water content at saturation ( $\theta_{sd}$ ) is 0.60–0.61 on average in soil 1 and soil 2, respectively. The value of parameter  $n_v$ , which affects the slope of the SWRC, varies from 1.40 to 1.80; parameter  $l$  ranges from −1 up to 1 in both the soils. The values of the parameters used for modeling the main drying curve agree with those obtained by Nicotera et al. [19], who tested several soil specimens sampled from the same layer (soils 1 and 2).

Regarding the main wetting curve, the parameter  $\theta_s^w$  is lower on average in soil 1 than in soil 2. The  $(\theta_s^w)/(\theta_s^d)$  ratio, which is an indicator of the fraction of entrapped air in the subsoil, varies from 0.85 to 0.98. The range of this ratio agrees with those reported in the literature for pyroclastic layers in other geological contexts in Campania: 0.72–0.95 [47,48]. However, the air volume that remains entrapped in the voids during the wetting process depends on a multiplicity of factors, such as pore size distribution, history of drying and wetting cycles, and water supply rate.

Soils 1 and 2 present a higher mean value of  $\alpha^w$  in the wetting branch with respect to the drying branch, as expected. The  $\alpha^w/\alpha^d$  ratio varies from 1.50 to 2.4 (Table 3), a range in agreement with that reported by Kool and Parker [41], which is  $2.08 \pm 0.46$  on average.

### 3.2. Investigation at the Medium Scale: Lysimeter

Figure 6 shows measured against predicted matric suctions and volumetric water contents at 50 cm for both the calibration stage (the first hydrological year, Figure 6a) and validation (the remaining three hydrological years, Figure 6b–d).

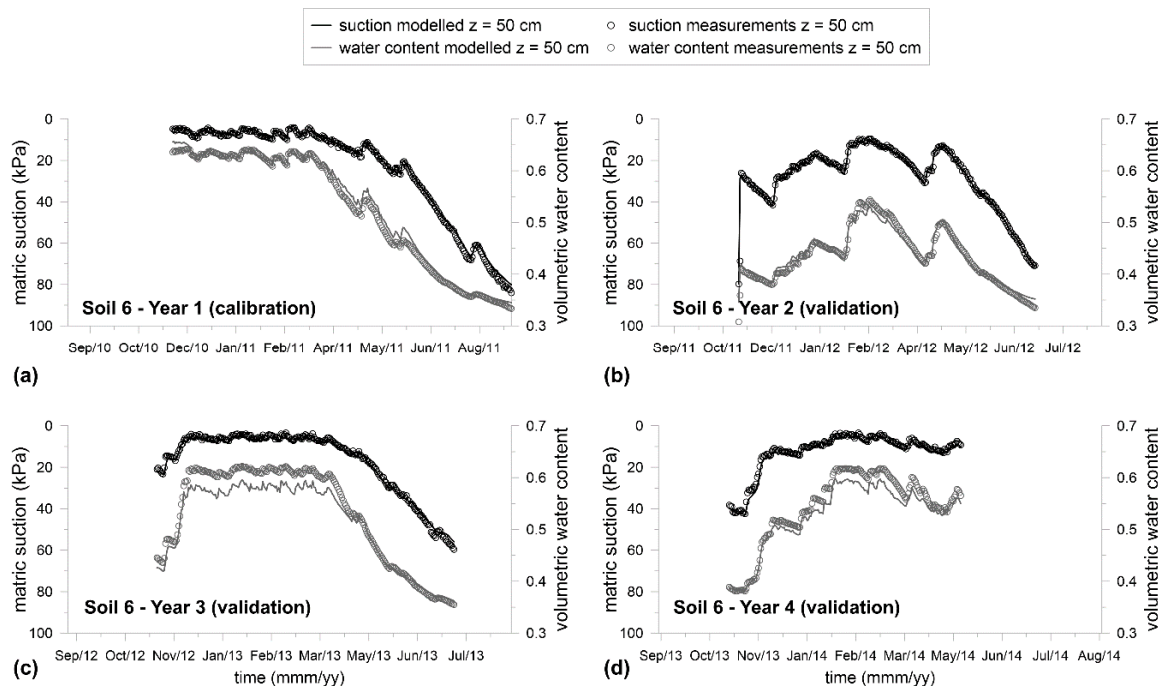


**Figure 6.** Results for soil 6 through monitoring by the lysimeter (medium scale). Experimental measurements of matric suction and volumetric water content at 50 cm (symbols) compared to the calculated values (continuous lines) by the model over time for soil 6 over the (a) first, (b) second, (c) third, and (d) fourth hydrological year of physical model monitoring. The first year was used for calibration, and the others were used for validation.

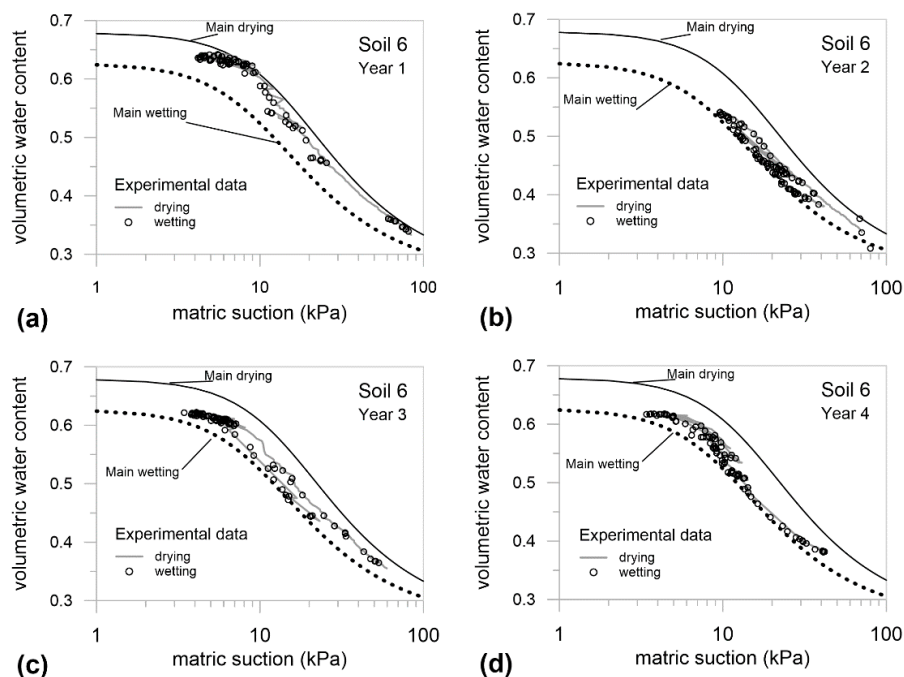
Regarding suction and water content measurements, it is noteworthy that, at each depth, the tensiometer and TDR probe (installed horizontally) were placed side by side. Nonetheless, the intrinsic differences between the two sensors, which, respectively, capture the response of a small vertical cylindrical soil volume (the tensiometer is 5 cm long and 2 cm wide) and of a larger roughly cylindrical horizontal volume (the TDR probe is 30 cm long), should be considered. The first sensor captures a local value, while the second probe measures an integral soil response. Finally, tensiometer measurements could be affected by a time-lag, depending on the hydraulic conductivity of the soil, while the time-lag could play a minor role for TDR probes. However, this last difference is usually considered negligible [49,50]. These considerations suggest critically assessing the exact values of the data, particularly if rapid variations are observed. In order to cope with such limitations, the analysis accounted for only measurements on a daily scale.

During the four hydrological years, the lysimeter was exposed to a variety of wetting and drying histories driven by the weather forcing evolutions typical of the Mediterranean area. Specifically, (1) precipitation patterns were characterized by rainy periods in autumn, winter, and early spring, and cumulative values decreased in the later spring and the summer months; and (2) temperature patterns were characterized by a decreasing trend from autumn to early winter, fluctuations around the lowest values occurred in winter, and a progressive increase that occurred up to a peak in summer.

Suction and volumetric water content measurements accounted for this seasonality of weather forcing. Regarding suction evolution, from late autumn to early spring, suction ranged from 20 to 4–5 kPa, with the lowest values occurring in winter. During the transition from the dry to the wet season

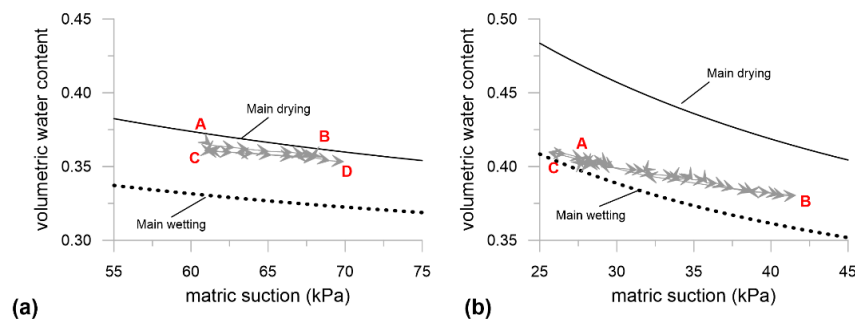
(April–June), and vice versa (October–November), suction ranged from 10 to about 50–60 kPa. During the dry periods (July–August–September), suction values rose above the Jet-fill’s full scale (70–80 kPa). The water content trends have patterns that are fully consistent with the suction trend, with the highest values occurring in winter. The range of variation is between 0.35 and 0.65. In general, the monitoring activity distinctly highlighted a peculiar history of experimental scanning paths throughout the investigated hydrological years, and most are well interpreted by the performed numerical analyses, either in wetting or in drying phases.

Figure 7 shows measured pairs of matric suction and volumetric water content at 50 cm in the SWRC plane. The figure also plots the main drying curve and main wetting curve determined by the calibration procedure (from the inverse analysis of the first hydrological year). The paths in part follow the main drying and wetting curves, the former during the calibration stage (Figure 7a) and the latter during the validation stage (Figure 7b,d). On the other hand, all pairs of experimental points fall in between the two main curves. From this perspective, it should be noted that most experimental paths cannot be uniquely recognized as the main drying or wetting curves, and the scanning curve’s slope seems to be slightly affected by the initial state and wetting/drying direction [47].



**Figure 7.** Results for soil 6 through monitoring by the lysimeter (medium scale). The main loop obtained from the inverse analysis of the first hydrological year (main drying and main wetting) overlaps with the experimental data recorded during the physical model monitoring over the (a) first, (b) second, (c) third, and (d) fourth hydrological year.

By enlarging the scale and looking at pairs of matric suction and volumetric water content to investigate hysteresis loops starting from different initial soil states (Figure 8), it should be noted that close hysteresis loops feature a limited internal hysteresis (Figure 8a,b) passing, in each case, through the reversal points (A~C), as stated by the LP model.



**Figure 8.** Experimental measurements of matric suction and volumetric water content at 50 cm (symbols) for hysteresis loops representative of different initial state conditions: (a) 20 July 2020–11 August 2011 (calibration period); (b) 08 November 2011–17 December 2011 (validation period).

Table 3 lists the Mualem–van Genuchten model parameters for soil 6, as carried out from the results of the optimization process of the first hydrological year [32]. Soil 6 features an intermediate behavior between coarse-grained and fine-grained materials. Its air-entry value (AEV) is about 15 kPa ( $\alpha^d = 0.07 \text{ kPa}^{-1}$ ), while the  $\alpha^w/\alpha^d$  ratio is 1.48 (Table 3), in line with the values reported by Kool and Parker [41]. Values of the  $(\theta_s^w)/(\theta_s^d)$  ratio ( $\sim 0.92$ ) reveal the presence of some entrapped air in the subsoil, in agreement with those reported in the literature for pyroclastic layers in other Campanian geological contexts (0.72–0.95) [48]. The estimation of the parameter  $\theta_s^w$  is also supported by the results of a full saturation test performed at the end of the fourth hydrological year (August 2014) for bare soil.

This saturation test was carried out by imposing on the exposed surface a water film acting as a zero-pressure condition, as long as the variations in weight due to surface water ponding were considered negligible. At the time of the start of the test, the matric suction values recorded in the layer were about 40–45 kPa. Figure 9 plots the pairs of matric suction–volumetric water content recorded at a depth of 50 cm. In this case, measurements were taken every 15 min. The figure also plots the main drying curve and main wetting curve, as well as the theoretical scanning wet paths carried out by using Equation (2) for different initial suction levels on the main drying curve. The experimental pairs run over the scanning wet paths, following the main wetting curve for matric suction values lower than 10 kPa and confirming the effectiveness of the estimated  $\theta_s^w$ .

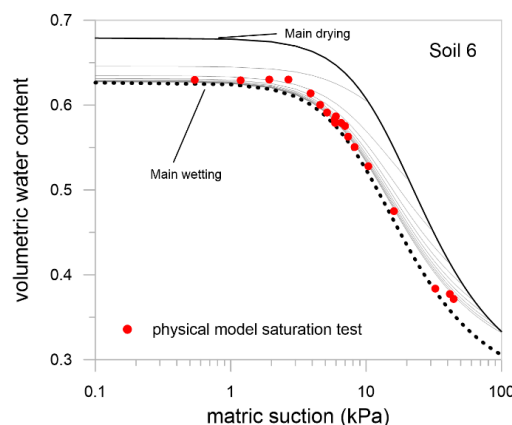


**Figure 9.** Comparison between the main loop obtained from the inverse analysis (main drying and main wetting) and the experimental data recorded during a full saturation test of the physical model performed at the end of the fourth hydrological year. Gray lines represent the theoretical paths determined by using Equation (2) for different initial suction levels on the main drying curve.

An overview of the capability of the hysteresis model of reproducing observed values is shown in Figure 10 by comparing the development over time of matric suction measurements with predictions

derived from observed water contents by taking hysteresis into account or ignoring it (in terms of main drying/wetting curve).

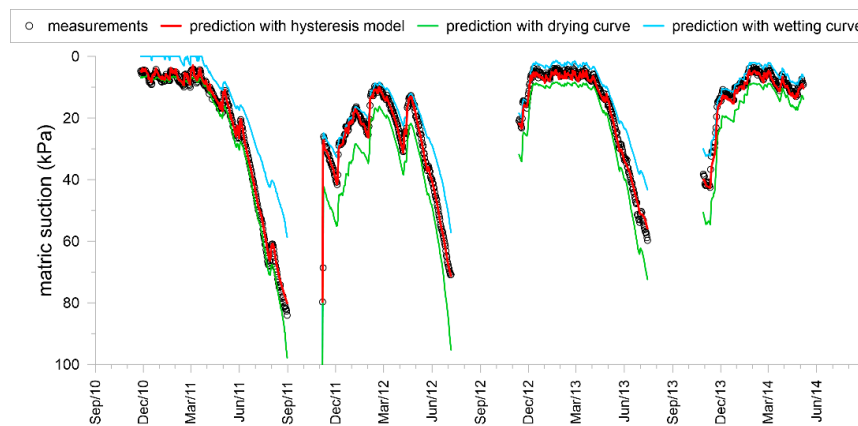


**Figure 10.** Evolution of matric suction measurements and theoretical predictions derived from water content measurements by using the LP model, main drying curve, and main wetting curve over 2010–2014.

This comparison reveals the performance of the LP model in reproducing satisfactory soil state variables related to slope stability and water stress in crops. The errors caused by ignoring hysteresis and the reduction of these errors by adopting the LP hysteresis model can also be appreciated quantitatively by evaluating the goodness of fit for matric suction via the Nash–Sutcliffe Efficiency (NSE [51]) and Kling–Gupta Efficiency (KGE [52]) indices (see Table 4). Briefly, NSE is defined as

$$NSE = \frac{\sum_{t=1}^T (V_{sim}(t) - V_{obs}(t))^2}{\sum_{t=1}^T (\overline{V_{obs}} - V_{obs}(t))^2}, \tag{5}$$

where  $V_{obs}(t)$  and  $V_{sim}(t)$ , respectively, represent the observed and simulated values at time  $t$ , while  $\overline{V_{obs}}$  represents the mean observed value. Values less than (equal to) zero indicate that the model is a worse (equivalent) predictor than the mean of the observations. The unit value indicates a perfect match between the model and observations. KGE is defined as

$$KGE = 1 - \sqrt{(r - 1)^2 + \left(\frac{\sigma_{sim}}{\sigma_{obs}} - 1\right)^2 + \left(\frac{\mu_{sim}}{\mu_{obs}} - 1\right)^2}, \tag{6}$$

where  $r$  represents the linear correlation between observations and simulations,  $\sigma$  is the standard deviation, and  $\mu$  is the mean value. In this case, the unit value also represents a perfect match, while the distinction between “good” and “bad” performances is highly debated in the literature [53].

**Table 4.** Values of Nash–Sutcliffe Efficiency (NSE) and Kling–Gupta Efficiency (KGE) for predictions via the LP hysteresis model, main drying, and main wetting curves.

NSE			KGE		
Hysteresis	Main Drying	Main Wetting	Hysteresis	Main Drying	Main Wetting
0.99	0.82	0.78	0.97	0.67	0.61

In general, satisfying results are achieved for the LP model (>0.95), while worse performances arise when considering the main drying and main wetting curves.

## 4. Discussion

### 4.1. Comparison between the LP Parameters Determined at Small/Medium Scales

In this section, a comparison between the model parameters determined for soils 1, 2, and 6 is carried out. By looking at the parameters of the LP model in Table 3, soil 1 and soil 2 are characterized by similar values of  $\theta_s^d$ ,  $\alpha^d$ ,  $\alpha^w$ , and  $n_v$ , with a value of  $l$  ranging between 0.5 and 1, probably due to an overlapping grain size distribution and some similarity in soil porosity. The mean value of  $\theta_s^w$  is different; however, in both cases, the ratio between  $\theta_s^w$  and soil porosity is in the range 0.83–0.84. The mean value of  $\theta_s^d$ ,  $n_v$  and  $\alpha^d$  for soil 6 are higher and lower than those obtained for soil 1 and soil 2, respectively. This is probably due to the higher fraction of fine soil and the higher porosity of soil 6 with respect to soil 1 and soil 2. For all the soils, the parameter values obtained by fitting the main wetting curve,  $\theta_s^w$  and  $\alpha^w$ , can be related, respectively, to porosity (coinciding with  $\theta_s^d$  if the soil starts from full saturation) and to the value of  $\alpha^d$  fitted along the main drying curve.

A hysteresis factor was also analytically quantified through the effective hysteresis indicator proposed by Gebrenegus and Ghezzehei [54], which computes the maximum deviation in effective saturation, ( $S_e = (\theta - \theta_r)/(\theta_s - \theta_r)$ ), between the two main curves. The computed value of this quantity is compared in Figure 11, with a cloud of experimental points provided by literature data from a wide spectrum of soils with different pore size distributions [55,56]. The points determined for soil 1, soil 2, and soil 6 are very close to one other and fall inside the cloud, indicating an intermediate behavior due to an intermediate pore size distribution (see Figure 2).

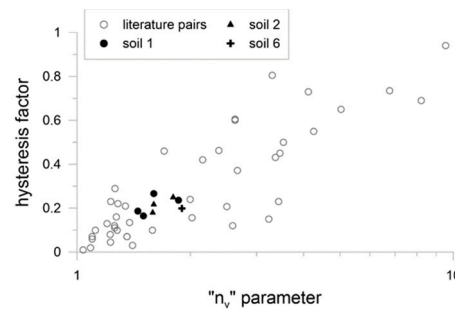


**Figure 11.** Hysteresis factor as a function of the parameter  $n_v$  of the Van Genuchten model. Hollow circles represent data provided by literature datasets, and filled-in symbols were values calculated in the present investigation.

### 4.2. Reliability of the Hydraulic Characterization Determined at Small/Medium Scales

In this section, a comparison between the main loop estimated by experimental data and the path detected by in situ measurements is carried out on the soil water retention plane in order to obtain an indication of the ability of the small- and medium-scale investigations to capture the hydraulic behavior actually observed in the field.

Field paths identified by coupling measurements of matric suction and volumetric water content collected at the same depth in soils 1, 2 and 6 every week over four years (2008–2012) are reported on the water retention plane in Figures 12–14; in each of these figures, there are also four enlargements of the water retention plane in which only data relating to a particular year of observation are shown (Figures 12b–e,g–l, 13b–d,g–l and 14b–d,g–l). The main loop obtained by inverse analyses (black continuous and black dotted lines) and the secondary wetting paths (gray dotted lines) determined by applying the LP model starting from different points on the main drying curve is also represented in Figures 12a,f, 13a,f, and 14a,f. In particular, the main loop was determined by adopting the mean values of fitting parameters for each soil (Table 3) in Equations (1) and (2).

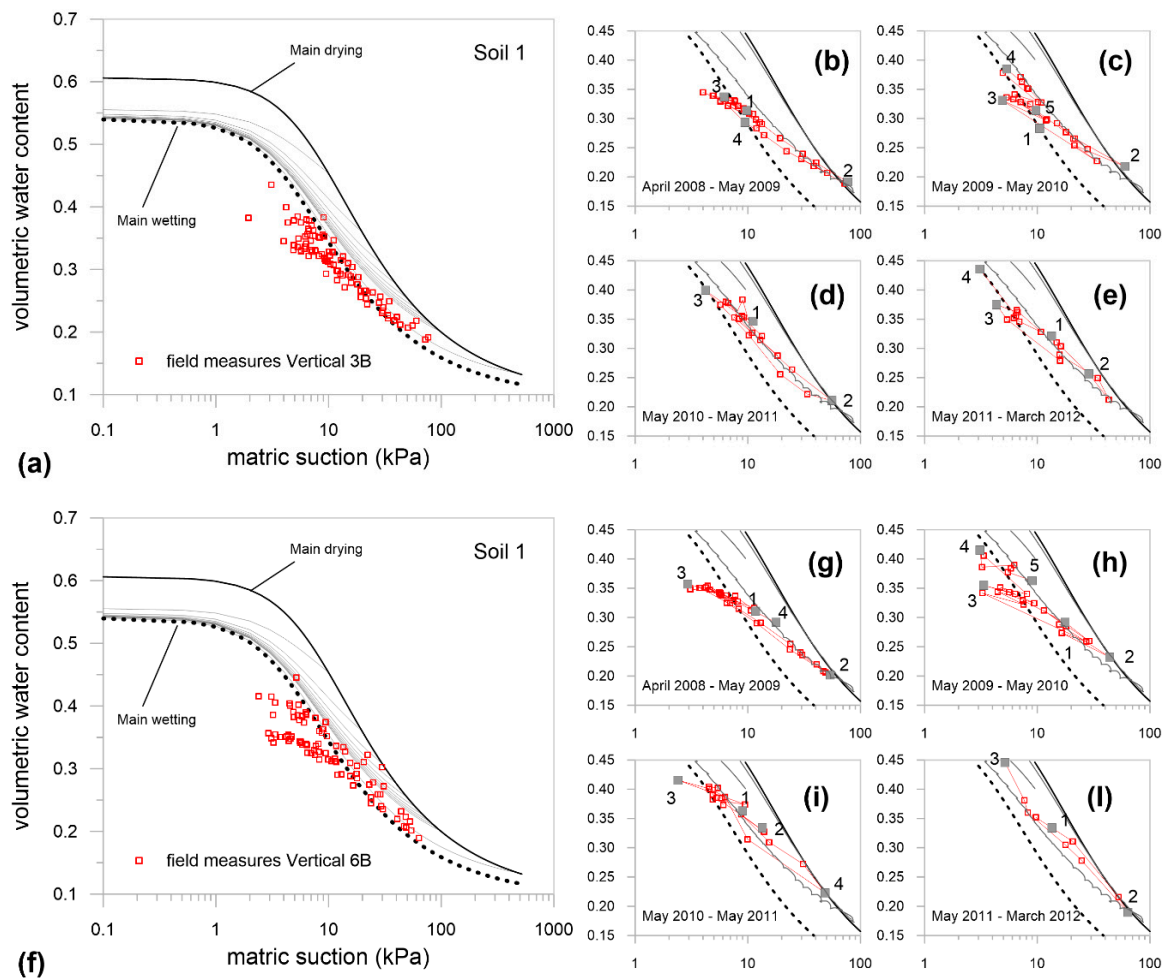


**Figure 12.** Pairs of matric suction and water content measurements collected at the site in soil 1 along verticals (a) 3B and (f) 6B compared to the main loop (continuous and dotted black lines) and to the secondary wetting paths starting from different points on the main drying curve (gray dotted lines). Field paths grouped by year and detected at vertical 3B (b–e) and at vertical 6B (g–l) compared to experimental path measured in the lab (test A).

By looking at Figures 12a,f, 13a,f, and 14a,f, the field paths detected in soil 1 and soil 2 cover a wider range of matric suction (between 2 kPa and 80 kPa), while those in soil 6 range between 3 kPa and 30 kPa. This is due to the different depths of installation from the ground surface.

The field paths look like scanning paths; the hysteresis can be clearly observed in the surficial soils only during the second year (May 2009–May 2010) by looking at paths 3–4 in Figure 12c,h. However, it is not possible to exactly follow the path due to the measurement frequency (one measurement per week), but it is clear that point 3 and point 4 are located on two different scanning curves. Then, the field paths identified in soil 1 very closely follow the cycles simulated in the lab, starting from the same initial point located on the main drying curve (see Figure 12b–e,g–l). Similar conclusions can be drawn by looking at the field paths identified in soil 6 and reported in Figure 14a–d for measurements collected along vertical 2B.

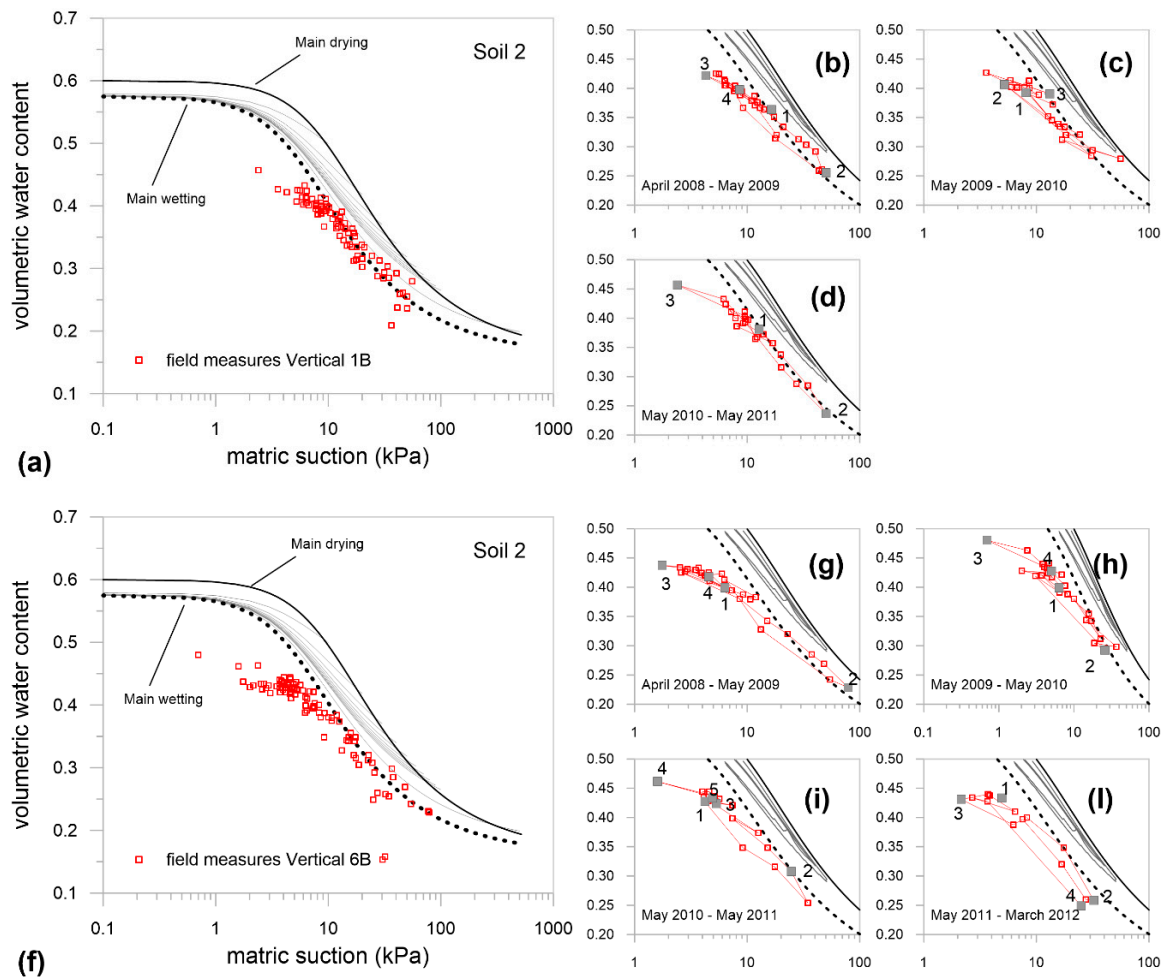


**Figure 13.** Pairs of matric suction and water content measurements collected at the site in soil 2 along verticals (a) 1B and (f) 6B compared to the main loop (continuous and dotted black lines) and to the secondary wetting paths starting from different points on the main drying curve (gray dotted lines). Field paths grouped by year and detected at vertical 1B (b–d) and at vertical 6B (g–i) compared to experimental path measured in the lab (test F).

More generally, some conclusions from the comparison between paths from the field and those modeled at small/medium scales can be drawn for all investigated soils:

1. Field paths are always distributed below the main drying curve determined by experimental investigation at small/medium scales (Figures 12a,f, 13a,f, and 14a,f);
2. Field paths mainly match the slope of the scanning paths determined by the LP model (see Figures 12b–e, 13g–i, and 14b–d);
3. Field paths, in some cases, exit the main loop determined at small/medium scales for suction below 10 kPa (see Figures 12g–i, 13b–d,g–i, and 14g–i); in other cases, they are included entirely in the loop (see Figures 12b–e and 14b–d).

Therefore, field and lab/lysimeter curves may be considered to be part of similar hysteresis loops, which differ according to the wetting procedure and history of wetting and drying phases. Therefore, scanning paths occurring at the site during wetting–drying cycles were quite well reproduced in both the physical prototype and soil specimen, at least up to 10 kPa.

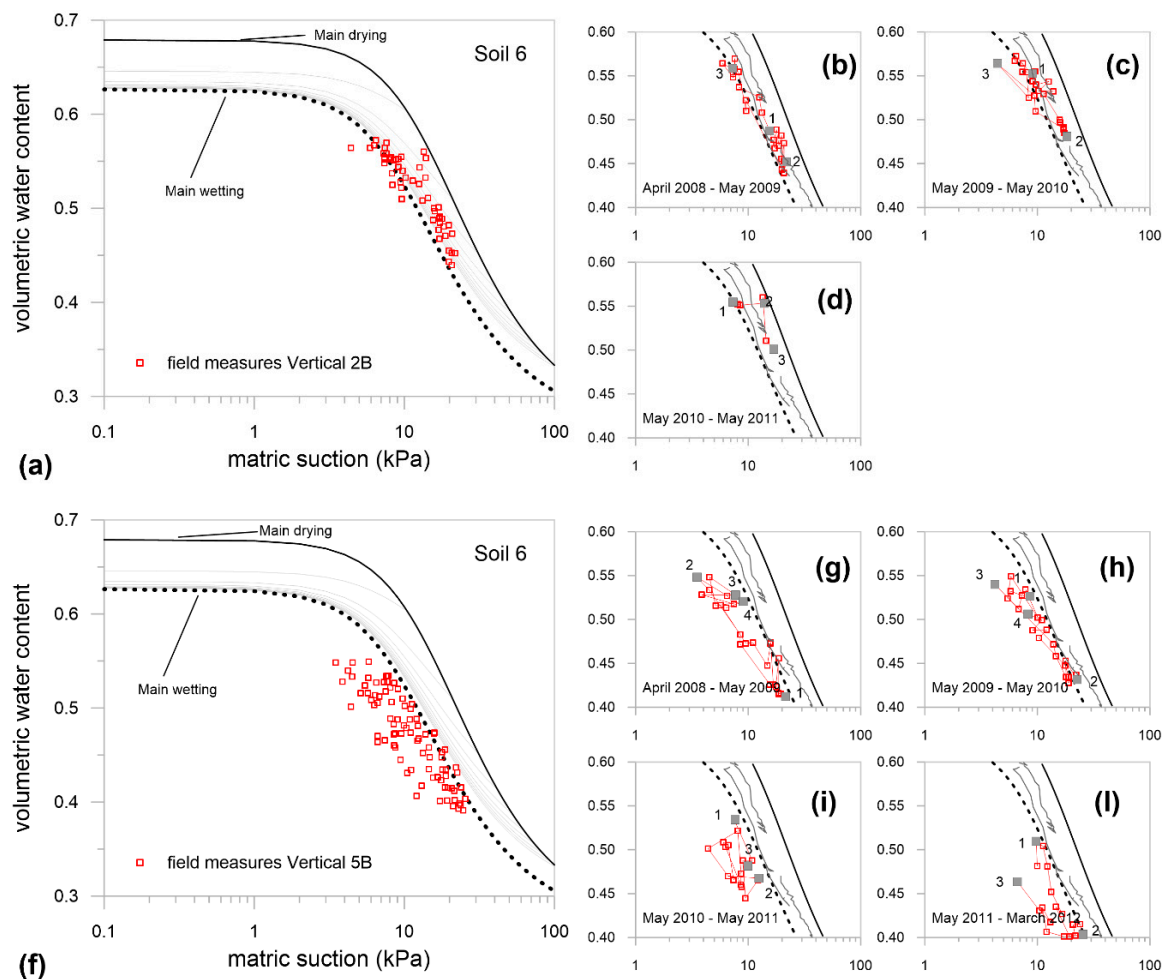


**Figure 14.** Pairs of matric suction and water content measurements collected at site in soil 6 along verticals (a) 2B and (f) 5B compared to the main loop (continuous and dotted black lines) and to the secondary wetting paths starting from different points on main drying curve (gray dotted lines). Field paths grouped by year and detected at vertical 2B (b–d) and at vertical 5B (g–l) compared to the experimental path measured in the physical model during the third monitoring year.

The observed differences between the field and lab/lysimeter results in the soil water retention plane, especially for matric suction lower than about 10 kPa, can be attributed to several factors, such as the discrepancy in the porosity among the soil volumes investigated at different scales, the size of the analyzed sample, and the ‘dynamic’ effects. The last one is associated with the apparent dependence of soil hydraulic properties on the flow dynamics, and this means that some difference in the SWRC can be observed for the same soil sample depending on the actual relative water flow velocity with respect to the solid skeleton and on the rate of variation in the saturation degree. The dynamic nonequilibrium of water flow in porous media is related to numerous phenomena, for instance, non-negligible resistance of air flow at high water saturation, microscopic redistribution of water and air phases, and local heterogeneities [9,10]. All these processes prevail in different suction ranges and on different time scales, and the practical impossibility of observing and quantifying them independently makes the modeling of water flow in porous media, including all aforementioned dynamic processes, very complex. Explicit modeling of two-phase flow and formulation of a ‘dynamic’ SWRC are required; some approaches for modeling dynamic nonequilibrium effects are reported in [9,10]. Nevertheless, simple modeling approaches consisting of the Richards equation with a ‘steady’ SWRC are often chosen for solving practical problems; for many years, these have been considered effective in treating these

phenomena from a macroscopic point of view, especially due to the lack of experimental evidence even from laboratory tests and to the difficulties in investigating the hydraulic hysteresis on site.

The amplitude of the hysteresis loop determined in the described tests is mainly related to the model parameter  $\theta_s^w$ , which is responsible for a loop that is so tight that it does not contain all paths observed in situ for matric suction lower than 10 kPa. However, as the match between the experimental data (from both the lab and lysimeter tests) and the results predicted by the LP model is very good (high value of  $R^2$ ), we can assume that the LP model also executes a good optimization of the parameter  $\theta_s^w$  if soil samples are also subject to different natural and artificial imbibition paths with very different infiltration rates or initial conditions. Summing up, even if the parameter  $\theta_s^w$  is not ‘a soil characteristic parameter’, the LP model is able to predict suction and water content in subsoils satisfactorily, at least at the scale of the data used for the model calibration (lab and lysimeter tests). On the contrary,  $\theta_s^w$ , as a result of the described fitting of the experimental data in the laboratory and from the lysimeter, does not always reproduce the hydraulic behavior observed in the field at a high degree of saturation. According to these considerations, the values of the parameter  $\theta_s^w$  seem to be primarily affected by the sample size and secondarily by the occurrence of the ‘dynamic effects’. The larger the modeled scale is, the more precise the determination of  $\theta_s^w$  could be.

In this regard, the values to assign to  $\theta_s^w$  in the LP model so that the main loop includes all the field paths were determined: 0.45 in soils 1 and 2; and 0.50 in soil 6. These values can be identified in Figure 15a–c, where the main loop and secondary scanning lines modeled by the LP model by keeping all the model parameters, apart from  $\theta_s^w$ , equal to the mean values determined by fitting the lab and lysimeter tests (Table 3) overlap with field data. These values correspond to a ratio,  $\theta_s^w/n$ , of 0.66 in soil 1, 0.68 in soil 2, and 0.72 in soil 6, close to the lower boundary, 0.72, reported in the literature [48] for this type of soil. In particular, some wetting paths measured at the site in soils 1, 2, and 6, chosen as examples, are reported in the zoom of Figure 15a–c. These paths are fit well by the wetting scanning lines (gray dotted lines) starting from the main drying at matric suction of 200 kPa for soil 1, of 250 kPa for soil 2, and of 75 and 30 kPa for soil 6 (path A–B and A’–B’, respectively) predicted by the LP model. The good agreement between the field wetting path and the secondary wetting curves of the LP model can also be appreciated quantitatively by evaluating the goodness of fit for measurements of volumetric water content at a fixed value of suction via Nash–Sutcliffe Efficiency (NSE [51]) and Kling–Gupta Efficiency (KGE [52]) indices (see Table 5).

**Table 5.** Values of Nash–Sutcliffe Efficiency (NSE) and Kling–Gupta Efficiency (KGE) for predictions of volumetric water content via the LP hysteresis model.

Material	Path	NSE	KGE
Soil 1	A–B	0.99	0.94
Soil 2	A–B	0.97	0.89
Soil 6	A–B	0.99	0.98
Soil 6	A’–B’	0.90	0.69

Therefore, when the field problem has to be modeled, inverse analyses should be carried out on paths detected by field measurements if these are available. Otherwise, according to the findings of this work, it is enough to use the model parameters determined by tests at small/medium scales and to measure the value of  $\theta_s^w$  in the field or to use a ratio of  $\frac{\theta_s^w}{n}$  equal to 0.70, on average, as a first approximation.

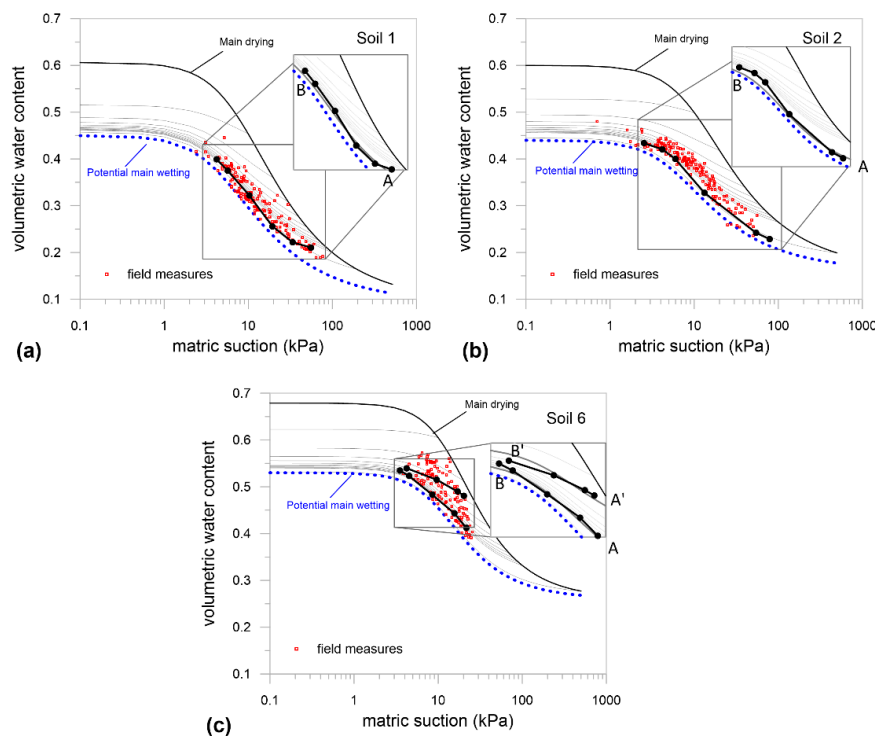


**Figure 15.** Pairs of matric suction and water content measurements collected at the site in soils 1 (a), 2 (b), and 6 (c) compared to the main loop (continuous and dotted blue lines) and to the secondary wetting paths starting from different points on the main drying curve (gray dotted lines) determined by the LP model. Examples of wetting field paths (circular black symbols connected by black lines) that overlap scanning wetting paths predicted by the LP model (gray dotted lines) are depicted in the zoom.

## 5. Conclusions

This paper reports the SWRCs for unsaturated pyroclastic soils obtained by using different experimental methods: lab tests on small specimens (small scale) and full instrumented lysimeter observations (medium scale). The values of parameters determined for all the soils agree with those reported in the literature for pyroclastic soils belonging to the Campania Region [8,16,19,57–61]. For the main wetting curve, the parameters  $\theta_s^w$  and  $\alpha^w$  can be related, respectively, to porosity and to  $\alpha^d$  values fitted along the main drying curve. The ratio between the value of  $\theta_s^w$  and soil porosity,  $n$ , ranges between 0.8 and 0.9, while  $\alpha^w/\alpha^d$  is between 1.5 (soil 6) and 2.4 (soils 1 and 2). The LP model satisfactorily reproduces the hydraulic soil response at small and medium scales.

In order to test the reliability of the hydraulic characterization determined at small/medium scales for modeling field problems, the main loop and secondary paths modeled for each tested soil were compared to the path obtained by coupling field measurements of matric suction and volumetric water content collected in the same soil layer. The major part of field paths matches the slope of the scanning paths determined by the LP model and is included entirely in the loop. Some field paths exit the main loop determined at small/medium scales for suction below 10 kPa, probably due to not having the proper value of the parameter  $\theta_s^w$ , indicating the amount of air entrapment. A proper parameter's assessment could require taking into account the sample size; then, a better estimation can be performed only by exploiting in situ measurements. However, as a first approximation, a ratio of  $\frac{\theta_s^w}{n}$  equal to 0.70 could be adopted.

Summing up, scanning paths occurring at the site during wetting–drying cycles are quite well reproduced in both the physical prototype and soil specimen, provided that the air entrapment value is well known.

**Author Contributions:** Methodology, all the authors; software analysis, M.P. and A.R.; in situ investigation, M.P., M.V.N., G.U.; laboratory test, M.V.N.; physical model investigation, L.P., G.R., and A.R.; data curation, M.P., G.R., and A.R.; Writing—Original Draft preparation, M.P.; Writing—Review and Editing, A.R., G.R., L.P., M.V.N., and G.U.; visualization, M.P. and A.R.; supervision, G.R., L.P., M.V.N., and G.U. All authors have read and agreed to the published version of the manuscript.

**Funding:** L.P. wishes to thank the ‘DIREZIONE NAZIONALE DIGHE’ which partly funded this project.

**Acknowledgments:** M.P. has partly developed this work within the framework of the project titled “New technologies for in time prediction of flowslide occurrence” (TEMPO). This project was carried out in the frame of Programme STAR, financially supported by UniNA and Compagnia di San Paolo.

**Conflicts of Interest:** The authors declare no conflict of interest.

## References

1. Toll, D.G.; Hughes, P.N.; Asquith, J.D. Soil water retention behaviour for an instrumented embankment. In Proceedings of the 3rd European Conference on Unsaturated Soils (E-UNSAT), Paris, France, 12–14 September 2016. [\[CrossRef\]](#)
2. Pirone, M.; Papa, R.; Nicotera, M.V.; Urciuoli, G. Hydraulic Behaviour of Unsaturated Pyroclastic Soil Observed at Different Scales. In Proceedings of the VI Italian Conference of Researchers in Geotechnical Engineering (CNRIG)—Geotechnical Engineering in Multidisciplinary Research: From Microscale to Regional Scale, Bologna, Italy, 22–23 September 2016.
3. Pirone, M.; Rianna, G.; Reder, A.; Pagano, L.; Urciuoli, G. Two Applications of Soil Water Balance in Unsaturated Pyroclastic Soils. In Proceedings of the VI Italian Conference of Researchers in Geotechnical Engineering, (CNRIG)—Geotechnical Engineering in Multidisciplinary Research: From Microscale to Regional Scale, Bologna, Italy, 22–23 September 2016.
4. Nielsen, D.R.; Van Genuchten, M.T.; Biggar, J.W. Water flow and solute transport process in the unsaturated zone. *Water Resour. Res.* **1986**, *22*, 89–108. [\[CrossRef\]](#)
5. De Rooij, G.H. Averaging hydraulic head, pressure head, and gravitational head in subsurface hydrology, and implications for averaged fluxes, and hydraulic conductivity. *Hydrol. Earth Syst. Sci.* **2009**, *13*, 1123–1132. [\[CrossRef\]](#)
6. Hopmans, J.W.; Nielsen, D.R. How useful are small-scale soil hydraulic property measurements for large-scale vadose zone modeling? In *Environmental Mechanics: Water, Mass and Energy Transfer in the Biosphere Geophysical Monograph*; American Geophysical Union: Washington, DC, USA, 2002. [\[CrossRef\]](#)
7. Papa, R.; Pirone, M.; Nicotera, M.V.; Urciuoli, G. Seasonal groundwater regime in an unsaturated pyroclastic slope. *Geotechnique* **2013**, *63*, 420–426. [\[CrossRef\]](#)
8. Comegna, L.; Damiano, E.; Greco, R.; Guida, A.; Olivares, L.; Picarelli, L. Field hydrological monitoring of a sloping shallow pyroclastic deposit. *Can. Geotech. J.* **2016**, *53*, 1125–1137. [\[CrossRef\]](#)
9. Durner, W.; Schultze, B.; Zurmühl, T. State-of-the-Art in Inverse Modeling of Inflow/Outflow Experiments. In Proceedings of the International Workshop on Characterization and Measurement of the Hydraulic Properties of Unsaturated Porous Media, University of California, Riverside, CA, USA, 22–24 October 1997; pp. 661–681.
10. Diamantopoulos, E.; Iden, I.C.; Durner, W. Inverse modeling of dynamic non-equilibrium in water flow with an effective approach. *Water Resour. Res.* **2012**, *48*, W03503. [\[CrossRef\]](#)
11. Pirone, M.; Papa, R.; Nicotera, M.V.; Urciuoli, G. In situ monitoring of the groundwater field in an unsaturated pyroclastic slope for slope stability evaluation. *Landslides* **2015**, *12*, 259–276. [\[CrossRef\]](#)
12. Pirone, M.; Papa, R.; Nicotera, M.V.; Urciuoli, G. Soil water balance in an unsaturated pyroclastic slope for evaluation of soil hydraulic behaviour and boundary conditions. *J. Hydrol.* **2015**, *528*, 63–83. [\[CrossRef\]](#)
13. Rianna, G.; Pagano, L.; Urciuoli, G. Investigation of soil–atmosphere interaction in pyroclastic soils. *J. Hydrol.* **2014**, *510*, 480–492. [\[CrossRef\]](#)
14. Reder, A.; Rianna, G.; Pagano, L. Physically based approaches incorporating evaporation for early warning predictions of rainfall-induced landslides. *Nat. Hazards Earth Syst. Sci.* **2018**, *18*, 613–631. [\[CrossRef\]](#)
15. Reder, A.; Rianna, G.; Pagano, L. Some aspects of water and energy budget of a pyroclastic cover. *Environ. Geotech.* **2019**, *6*, 406–419. [\[CrossRef\]](#)
16. Pagano, L.; Reder, A.; Rianna, G. Effects of vegetation on hydrological response of silty volcanic covers. *Can. Geotech. J.* **2019**, *56*, 1261–1277. [\[CrossRef\]](#)

17. Parker, J.C.; Lenhard, R.J. A Model for Hysteretic Constitutive Relations Governing Multiphase Flow 1. Saturation Pressure Relations. *Water Resour. Res.* **1987**, *23*, 2187–2196. [CrossRef]
18. Van Genuchten, M.T. A Closed-Form Equation for Predicting the Hydraulic Conductivity of Unsaturated Soils. *Soil Sci. Soc. Am. J.* **1980**, *44*, 892–898. [CrossRef]
19. Nicotera, M.V.; Papa, R.; Urciuoli, G. An experimental technique for determining the hydraulic properties of unsaturated pyroclastic soils. *Geotech. Test. J.* **2010**, *33*, 263–285. [CrossRef]
20. Pirone, M.; Urciuoli, G. Cyclical suction characteristics in unsaturated slopes. In Proceedings of the International Workshop on Volcanic Rocks and Soils, Ischia Island, Italy, 24–25 September 2015; pp. 183–185.
21. Schaap, M.G.; Van Genuchten, M.T. A Modified Mualem–van Genuchten Formulation for Improved Description of the Hydraulic Conductivity Near Saturation. *Vadose Zone J.* **2006**, *5*, 27–34. [CrossRef]
22. Tarantino, A. A water retention model for deformable soils. *Geotechnique* **2009**, *59*, 751–762. [CrossRef]
23. Pasha, A.Y.; Khoshghalb, A.; Khalili, N. Hysteretic model for the evolution of water retention curve with void ratio. *ASCE's J. Eng. Mech.* **2017**, *143*. [CrossRef]
24. Gallipoli, D.; Wheeler, S.J.; Karstunen, M. Modelling the variation of degree of saturation in a deformable unsaturated soil. *Geotechnique* **2003**, *53*, 105–112. [CrossRef]
25. Pasha, A.Y.; Khoshghalb, A.; Khalili, N. Can degree of saturation decrease during constant suction compression of an unsaturated soil? *Comput. Geotech.* **2019**, *106*, 199–204. [CrossRef]
26. Khoshghalb, A.; Pasha, A.Y.; Khalili, N. A Fractal Model for Volume Change Dependency of the Water Retention Curve. *Géotechnique* **2015**, *62*, 141–146. [CrossRef]
27. Nuth, M.; Laloui, L. Advances in modelling hysteretic water retention curve in deformable soils. *Comput. Geotech.* **2008**, *35*, 835–844. [CrossRef]
28. Pasha, A.; Khoshghalb, A.; Khalili, N. Evolution of isochoric water retention curve with void ratio. *Comput. Geotech.* **2020**, *122*, 103536. [CrossRef]
29. Pasha, A.Y.; Khoshghalb, A.; Khalili, N. Pitfalls in Interpretation of Gravimetric Water Content–Based Soil–Water Characteristic Curve for Deformable Porous. *Int. J. Geomech.* **2016**, *16*, D4015004. [CrossRef]
30. Nicotera, M.V.; Papa, R.; Urciuoli, G. The Hydro-Mechanical Behaviour of Unsaturated Pyroclastic Soils: An Experimental Investigation. *Eng. Geol.* **2015**, *195*, 70–84. [CrossRef]
31. Papa, R. Indagine Sperimentale sulla Coltre Piroclastica di un Versante della Campania [Experimental investigation on the pyroclastic cover of a slope in Campania (Italy)]. Ph.D. Thesis, Università di Napoli Federico II, Napoli, Italy, 2007; p. 367.
32. Pagano, L.; Picarelli, L.; Rianna, G.; Urciuoli, G. A simple numerical procedure for timely prediction of precipitation-induced landslides in unsaturated pyroclastic soils. *Landslides* **2010**, *7*, 273–289. [CrossRef]
33. Lo Presti, D.C.F.; Pedroni, S.; Crippa, V. Maximum dry density of cohesionless soil by pluviation and by ASTM D 4253–83: A comparative study. *Geotech. Test. J.* **1992**, *15*, 180–189.
34. Reder, A.; Pagano, L.; Picarelli, L.; Rianna, G. The role of the lowermost boundary conditions in the hydrological response of shallow sloping covers. *Landslides* **2017**, *14*, 861–873. [CrossRef]
35. Lenhard, R.J.; Parker, J.C.; Kaluarachchi, J.J. Comparing Simulated and Experimental Hysteretic Two-Phase Transient Fluid Phenomena. *Water Resour. Res.* **1991**, *27*, 2113–2124. [CrossRef]
36. Lenhard, R.J.; Parker, J.C. A Model for Hysteretic Constitutive Relations Governing Multiphase Flow 2. Permeability–Saturation Relations. *Water Resour. Res.* **1987**, *23*, 2187–2196. [CrossRef]
37. Dias, A.S. The Effect of Vegetation on Slope Stability of Shallow Pyroclastic Soil Covers. Ph.D. Thesis, University of Montpellier, Montpellier, France, 2019. Available online: <https://tel.archives-ouvertes.fr/tel-02045922> (accessed on 25 January 2019).
38. Ippisch, O.; Vogel, H.-J.; Bastian, P. Validity limits for the van Genuchten–Mualem model and implications for parameter estimation and numerical simulation. *Adv. Water Resour.* **2006**, *29*, 1780–1789. [CrossRef]
39. Madi, R.; De Rooij, G.H.; Mielenz, H.; Mai, J. Parametric soil water models: A critical evaluation of expressions for the full moisture range. *Hydrol. Earth Syst. Sci.* **2018**, *22*, 1193–1219. [CrossRef]
40. Scott, P.S.; Farquhar, G.J.; Kouwen, N. Hysteretic effects on net infiltration. *Advances in Infiltration. Am. Soc. Agric. Eng. Publ.* **1983**, *11–83*, 163–170.
41. Kool, J.B.; Parker, J.C. Development and Evaluation of Closed-form Expressions for Hysteretic Soil Hydraulic Properties. *Water Resour. Res.* **1987**, *23*, 105–114. [CrossRef]
42. Werner, A.D.; Lockington, D.A. Artificial pumping errors in the Kool–Parker scaling model of soil moisture hysteresis. *J. Hydrol.* **2006**, *325*, 118–133. [CrossRef]

43. Land, C.S. Calculation of Imbibition Relative Permeability for Two-and Three-Phase Flow from Rock Properties. *Soc. Pet. Eng. J.* **1968**, *8*, 149–156. [[CrossRef](#)]
44. Mualem, Y. A modified dependent-domain theory of hysteresis. *Soil Sci.* **1984**, *137*, 283–291. [[CrossRef](#)]
45. Šimůnek, J.; Šejna, M.; Saito, H.; Sakai, M.; Van Genuchten, M.T. *The HYDRUS-1D Software Package for Simulating the One-Dimensional Movement of Water, Heat, and Multiple Solutes in Variably-Saturated Media* 2013, Technical manual, version 4.16; Department of Environmental Science University of California Riverside: Riverside, CA, USA, 2013.
46. Marquard, D.W. An Algorithm for Least-Squares Estimation of Nonlinear Parameters. *J. Soc. Ind. Appl. Math.* **1963**, *11*, 431–441. [[CrossRef](#)]
47. Rianna, G.; Comegna, L.; Pagano, L.; Picarelli, L.; Reder, A. The Role of Hydraulic Hysteresis on the Hydrological Response of Pyroclastic Silty Covers. *Water* **2019**, *11*, 628. [[CrossRef](#)]
48. Basile, A.; Ciollaro, G.; Coppola, A. Hysteresis in Soil Water Characteristics as a Key to Interpreting Comparisons of Laboratory and Field Measured Hydraulic Properties. *Water Resour. Res.* **2003**, *39*, 1355. [[CrossRef](#)]
49. Askarinejad, A.; Casini, F.; Kienzler, P.; Springman, S.M. Comparison of the in situ and laboratory water retention curves for a silty sand. In Proceedings of the 5th International Conference of Unsaturated Soils (UNSAT), Barcelona, Spain, 6–9 September 2011.
50. Ng, C.W.W.; Wong, H.N.; Tse, Y.M.; Pappin, J.W.; Sun, H.W.; Millis, S.W.; Leung, A.K. A field study of stress-dependent soil–water characteristic curves and permeability of a saprolitic slope in Hong Kong. *Geotechnique* **2011**, *61*, 511–521. [[CrossRef](#)]
51. Nash, J.E.; Sutcliffe, J.V. River flow forecasting through conceptual models, Part I: A discussion of principles. *J. Hydrol.* **1970**, *10*, 282–290. [[CrossRef](#)]
52. Gupta, H.V.; Kling, H.; Yilmaz, K.K.; Martinez, G.F. Decomposition of the mean squared error and NSE performance criteria: Implications for improving hydrological modelling. *J. Hydrol.* **2009**, *377*, 80–91. [[CrossRef](#)]
53. Knoben, W.J.M.; Freer, J.E.; Woods, R.A. Technical note: Inherent benchmark or not? Comparing Nash–Sutcliffe and Kling–Gupta efficiency scores. *Hydrol. Earth Syst. Sci.* **2019**, *23*, 4323–4331. [[CrossRef](#)]
54. Gebrenegus, T.; Ghezzehei, T.A. An index for degree of hysteresis in water retention. *Soil Sci. Soc. Am. J.* **2011**, *75*, 2122–2127. [[CrossRef](#)]
55. Yang, C.; Sheng, D.; Carter, J.P. Effect of Hydraulic Hysteresis on Seepage Analysis for Unsaturated Soils. *Comput. Geotech.* **2012**, *41*, 36–56. [[CrossRef](#)]
56. Huang, H.C.; Tan, Y.C.; Liu, C.W.; Chen, C.H. A novel hysteresis model in unsaturated soil. *Hydrol. Process.* **2005**, *19*, 1653–1665. [[CrossRef](#)]
57. Capparelli, G.; Spolverino, G. An Empirical Approach for Modeling Hysteresis Behavior of Pyroclastic Soils. *Hydrology* **2020**, *7*, 14. [[CrossRef](#)]
58. Greco, R.; Comegna, L.; Damiano, E.; Guida, A.; Olivares, L.; Picarelli, L. Hydrological modelling of a slope covered with shallow pyroclastic deposits from field monitoring data. *Hydrol. Earth Syst. Sci.* **2013**, *17*, 4001–4013. [[CrossRef](#)]
59. Santo, A.; Di Crescenzo, G.; Forte, G.; Papa, R.; Pirone, M.; Urciuoli, G. Flow-type landslides in pyroclastic soils on flysch bedrock in southern Italy: The Bosco de’ Preti case study. *Landslides* **2018**, *15*, 63–82. [[CrossRef](#)]
60. Forte, G.; Pirone, M.; Santo, A.; Nicotera, M.V.; Urciuoli, G. Triggering and predisposing factors for flow-like landslides in pyroclastic soils: The case study of the Lattari Mts. (southern Italy). *Eng. Geol.* **2019**, *257*, 105137. [[CrossRef](#)]
61. Pirone, M.; Papa, R.; Nicotera, M.V.; Urciuoli, G. Analysis of Safety Factor in unsaturated pyroclastic slope. In *Landslides and Engineered Slopes. Experience, Theory and Practice*; CRC Press: Naples, Italy, 2016; Volume 3, pp. 1647–1654. [[CrossRef](#)]

